ACS APPLIED MATERIALS & INTERFACES

www.acsami.org

Research Article

NIR-Responsive Lysosomotropic Phototrigger: An "AIE + ESIPT" Active Naphthalene-Based Single-Component Photoresponsive Nanocarrier with Two-Photon Uncaging and Real-Time Monitoring Ability

Biswajit Roy, Rakesh Mengji, Samrat Roy, Bipul Pal, Avijit Jana,* and N. D. Pradeep Singh*

Cite This: *ACS Appl. Mater. Interfaces* 2022, 14, 4862−4870

Read Online

ACCESS | Metrics & More | Article Recommendations | Supporting Information

ABSTRACT: In recent times, organelle-targeted drug delivery systems have gained tremendous attention due to the site-specific delivery of active drug molecules, resulting in enhanced bioefficacy. In this context, a phototriggered drug delivery system (DDS) for releasing an active molecule is superior, as it provides spatial and temporal control over the release. So far, a near-infrared (NIR) light-responsive organelle-targeted DDS has not yet been developed. Hence, we introduced a two-photon NIR light-responsive lysosome-targeted "AIE + ESIPT" active single-component DDS based on the naphthalene chromophore. The two-photon absorption cross section of our DDS is 142 GM at 850 nm. The DDS was converted into pure organic nanoparticles for biological applications. Our nano-DDS is capable of selective targeting, AIE luminogenic imaging, and drug release within the lysosome. *In vitro* studies using cancerous cell lines showed that our single-component photoresponsive nanocarrier exhibited enhanced cytotoxicity and real-time monitoring ability of drug release.

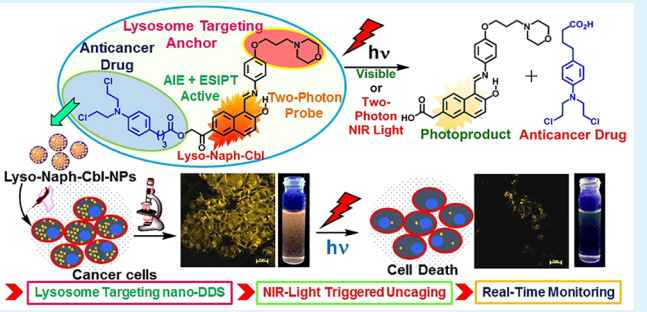

KEYWORDS: *lysosome targeting, drug delivery system, nanoparticle, two-photon uncaging, AIE, ESIPT*

INTRODUCTION

Lysosomes were discovered in 1955 by Christian de Duve.[1] They are single membranous subcellular organelles and ubiquitous in almost all eukaryotic cells.[2] Lysosomes play essential roles in digestion, foreign substance scavenging, and autophagy to maintain cellular homeostasis.[3] The acidic environment (pH 4.5−5.5) of lysosomes helps digest all types of macromolecules.[2,3] Disruption of lysosomal functions leads to several diseases. Fifty types of monogenic diseases are related to lysosomal dysfunction. Most of them fall in the category of lysosomal storage diseases (LSDs). Other important diseases are Alzheimer's disease, autoimmune diseases, and resistance to autoimmune diseases.[4] When the lysosomal degradative pathway gets dysregulated, diseases like cancer are known to progress.[5]

Researchers have recently focused on developing lysosome-targeted drug delivery systems (DDSs) mainly because many of the drug molecules need to be specifically localized in the lysosome to exhibit their maximum activity.[4] Further, several drugs suffer from multidrug resistance (MDR) due to lysosomal autophagy.[6,7] Importantly, targeting the lysosome ensures facile intercellular drug release. Because of these reasons, lysosomes become a vital organelle for targeted drug delivery.[3] Hence, several pH-responsive and enzyme-responsive drug delivery systems were reported, which specifically released the drug within the lysosome due to its acidic and enzyme-enriched environment.[8−12] However, these delivery systems lack control over the drug uncaging process. In this context, light-triggered DDSs have gained considerable importance in the last few decades because they provide high spatiotemporal control over drug release.[13]

Recently, lysosome-targeted light-responsive DDSs based on coumarin[14] and the BODIPY[15] chromophore have been reported. Riezman et al. developed for the first time a lysosome-targeted coumarin-based DDS to uncage sphingosine, a lipid molecule, by UV light illumination.[14] They investigated the localization-dependent metabolism of the lipid molecule and found a distinct metabolic pattern of lysosomal sphingosine. Later, Weinstain et al. reported several organelle-targeted visible light-responsive photocages based on the meso-methyl BODIPY backbone.[15] They discovered that the

Received: October 4, 2021
Accepted: January 6, 2022
Published: January 20, 2022

Scheme 1. Working Protocol of Lyso-Naph-Cbl

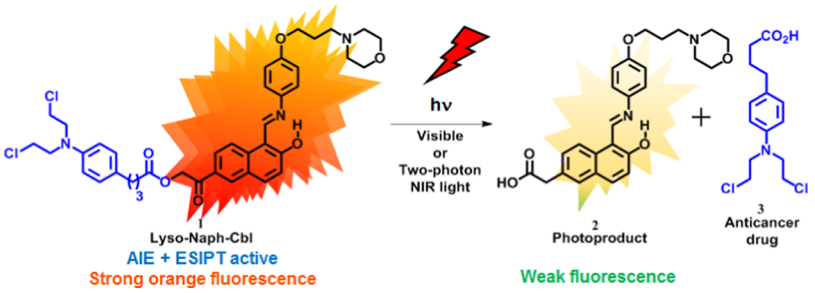

Scheme 2. Synthesis of Lyso-Naph-Cbl[a]

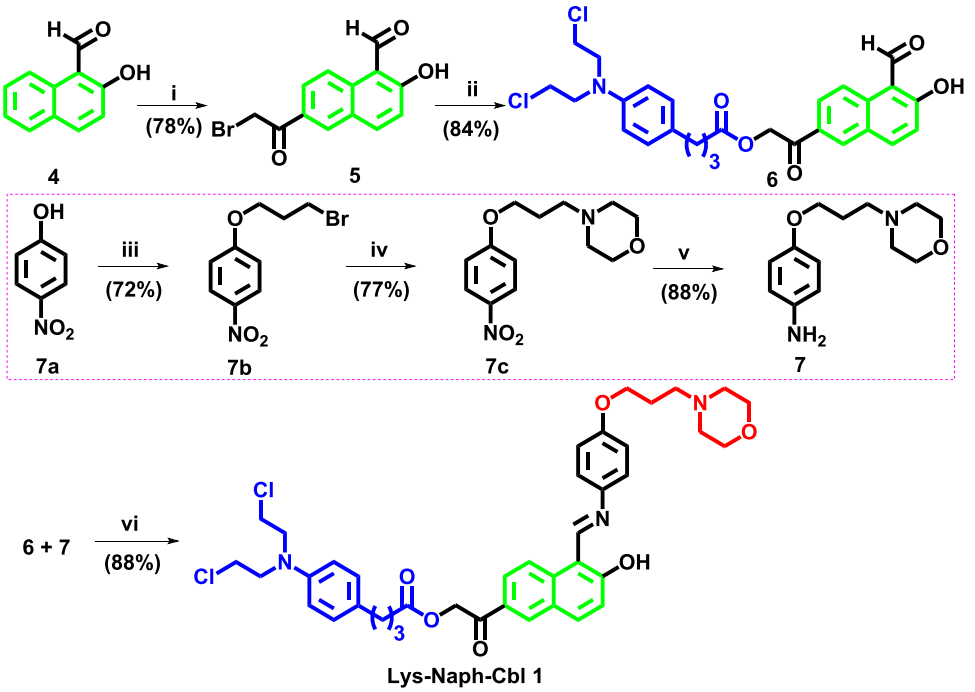

[a]Reaction condition: (i) bromoacetyl bromide, $AlCl_3$, dry DCM, 0 °C, 5 h; (ii) chlorambucil, K_2CO_3, acetonitrile, rt, 4 h; (iii) 1,3-dibromopropane, K_2CO_3, dry dimethyl sulfoxide (DMSO), 70 °C, 4 h; (iv) morpholine, K_2CO_3, dry DMSO, 80 °C, 5 h; (v) $SnCl_2{\cdot}2H_2O$, EtOAc, reflux, 3 h; and (vi) dry benzene, Dean−Stark, 4 h.

predesigned photocages exhibit organelle-specific localization and higher efficacy of the active molecule upon release.

To date, a near-infrared (NIR) light-responsive organelle targetable DDS has not been developed. By any means, if we can develop an NIR-responsive organelle targetable DDS, we can improve the drug efficacy and eliminate the competitive absorptions of light by natural pigments like hemoglobin. As we know, light below 650 nm is primarily absorbed by hemoglobin.[13] Hence, we intend to design a two-photon responsive lysosomotropic DDS that can be operated in the NIR region. With two-photon excitation, the active molecule can be released only at the focal point of the laser, which enables three-dimensional control over uncaging with high spatial and temporal precision.[16,17]

Herein, we designed a lysosome-targeted two-photon responsive "aggregation-induced emission (AIE) + excited-state intramolecular proton transfer (ESIPT)" active single chromophoric drug delivery system (Scheme 1), named lysosomotropic-naphthalene-chlorambucil conjugate (Lyso-Naph-Cbl **1**). Lyso-Naph-Cbl consists of a two-photon active 2-hydroxy-6-napthacyl backbone[18] assembled with an imine sidearm at 1-position of naphthalene and caged alkylating agent chlorambucil. Our DDS (Lyso-Naph-Cbl) exhibits the following advantages: (i) due to the presence of an imine linker, the adjacent hydroxyl group takes part in the ESIPT process[19−21] and also persuades the AIE property,[22−25] thereby providing better visualization; (ii) targets lysosome due to the installed morpholine moiety, which acts as a lysosomotropic anchor;[3] (iii) releases the drug molecule upon single-photon excitation by visible light irradiation as well as upon two-photon excitation with NIR light irradiation; and (iv) capable of monitoring drug release in real time by a sharp decrease in fluorescence intensity.

RESULTS AND DISCUSSION

Synthesis of Lyso-Naph-Cbl. We synthesized our DDS starting from commercially available 2-hydroxy-1-naphthaldehyde (**4**). Friedel−Crafts acylation on **4** with bromoacetyl bromide in the presence of $AlCl_3$ gave compound **5**. Bromo derivative **5** was then esterified with chlorambucil using K_2CO_3 as a base in acetonitrile to furnish compound **6**. Then, to attach the sidearm at 1-position, we separately synthesized amine

https://doi.org/10.1021/acsami.1c19022
ACS Appl. Mater. Interfaces 2022, 14, 4862−4870

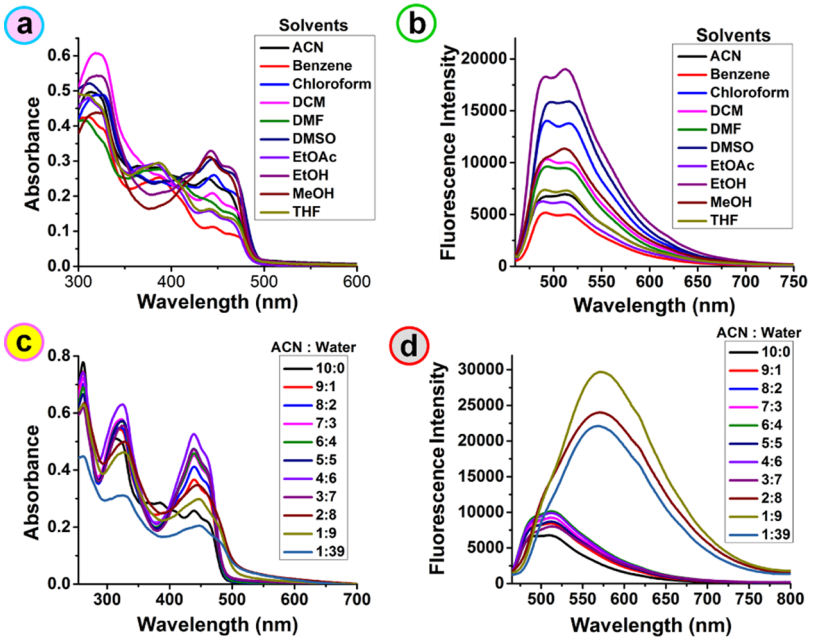

Figure 1. (a) UV−vis absorbance and (b) fluorescence spectra of Lys-Naph-Cbl (1×10^{-5} M) in different solvents. (c) UV−vis absorbance and (d) fluorescence spectra of Lyso-Naph-Cbl (1×10^{-5} M) in acetonitrile−water binary mixtures with varying proportions.

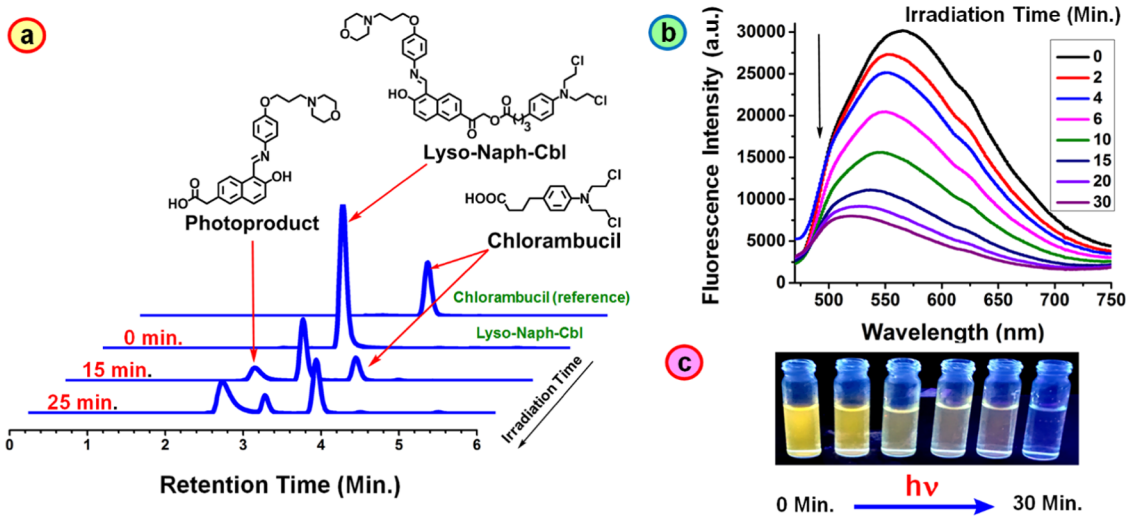

Figure 2. (a) HPLC overlay chromatogram of Lyso-Naph-Cbl at different time intervals of light irradiation (≥410 nm). (b) Change in the fluorescence spectral profile of Lyso-Naph-Cbl with increasing irradiation time. (c) Change in the fluorescence intensity during the course of photolysis of Lyso-Naph-Cbl observed under a UV lamp (365 nm) by the naked eye.

compound **7** starting with 4-nitrophenol (7a) following the known procedure[26] (Scheme 2). Then, compounds **6** and **7** were condensed via Dean−Stark distillation in benzene to afford our DDS Lyso-Naph-Cbl **1**. All the synthesized compounds were characterized using ^{1}H NMR, ^{13}C NMR, and HRMS (see pages S5−17 in the Supporting Information).

Photophysical Properties of Lyso-Naph-Cbl. The photophysical properties of Lyso-Naph-Cbl were investigated in different solvents (Figure 1). The results showed that Lyso-Naph-Cbl exhibited two absorption maxima due to the ESIPT process.[19−21] Absorption maxima at 390 and 460 nm corresponds to the keto form and enol form of Lyso-Naph-Cbl (Figure 1a), respectively. However, we noted the absorption maximum corresponding to the enol form to be intense in polar protic solvents. Next, we recorded the emission spectra of Lyso-Naph-Cbl and noted two different emission maxima at 480 and 530 nm (Figure 1b).

To demonstrate the AIE property of our DDS, we recorded the fluorescence intensity of Lyso-Naph-Cbl in acetonitrile buffer (pH 7.4) binary mixtures (Figure 1c,d) with varying water fractions (f_w). Initially, Lyso-Naph-Cbl showed green fluorescence in pure acetonitrile that, upon increasing the water fraction (f_w < 80%), became intense, which corresponds to the emission of the high-energy enol form, which predominates in the solution state with a small Stokes shift of 60 nm (Figure 1d). With further increase of the water fraction above 80−97%, the emission maximum exhibited a 6 times enhancement in fluorescence intensity, proving the presence of the AIE property.[22−25] Interestingly, we observed a large Stokes shift of around 195 nm at f_w > 80%, which

https://doi.org/10.1021/acsami.1c19022
ACS Appl. Mater. Interfaces 2022, 14, 4862−4870

Scheme 3. Possible Photorelease Mechanism of Lyso-Naph-Cbl

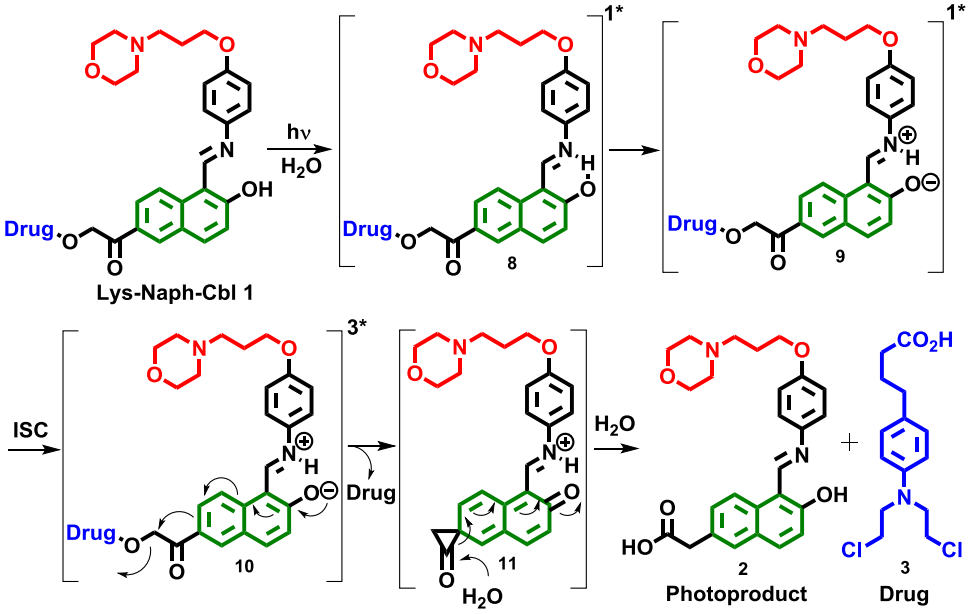

corresponds to the low-energy keto form that predominates in the aggregated state (λ_{em} = 575 nm). We also recorded the solid-state fluorescence spectrum of Lyso-Naph-Cbl to confirm the predominance of the keto form in the solid state (Figure S16).

Stability of Lyso-Naph-Cbl. We recorded the ^{1}H NMR of Lyso-Naph-Cbl in a DMSO-d_6 and D_2O mixture to check the hydrolytic stability of the imine bond of Lyso-Naph-Cbl (Figure S17). From Figure S17, we noted that <5% Lyso-Naph-Cbl decomposes after 3 days. Further, we checked the stability of Lyso-Naph-Cbl in a biological medium and two other pH values (5.4 and 8) at 37 °C under dark conditions. From Table S1, we observed that no significant amount of drug was released by our DDS after 7 days.

Photouncaging of Chlorambucil from Lyso-Naph-Cbl. To check that our DDS can release caged chlorambucil upon light irradiation, we investigated its single-photon uncaging ability and the quantum yield of the photorelease. A 40 mL (1×10^{-4} M) solution of Lyso-Naph-Cbl in (f_w = 95%) ACN/PBS buffer (pH = 7.4) mixture was irradiated with visible light ($\lambda \geq 410$ nm) from a 125 W medium pressure mercury lamp as the light source using a 1 M solution of $NaNO_2$ as the UV cutoff filter. We monitored the photouncaging process by reverse-phase high-performance liquid chromatography (RP-HPLC) and emission spectroscopy. From the RP-HPLC diagram (Figure 2a), we observed that the peak at t_R (retention time) = 3.2 gradually decreased, indicating the photodecomposition of Lyso-Naph-Cbl. On the other hand, we noted a continuous increase of two new peaks at t_R = 2.8 and 3.8, indicating photoproduct formation and uncaged chlorambucil. Figure 2a shows that 90% of the drug was released by DDS in 25 min of irradiation (Figure S18a). To check that the uncaging process depends only upon light irradiation, we performed the photouncaging process in the presence and absence of light. Figure S18b shows that photouncaging of chlorambucil is solely dependent on light irradiation.[18,27]

Next, we recorded the emission spectra during photolysis. Interestingly, we noted a sharp decrease in the emission maximum during photouncaging. Initially, our DDS exhibited bright orange fluorescence, and after 25 min of irradiation, DDS showed faint fluorescence. The initial peak at 575 nm of DDS gradually decreased, and a five times decrease in fluorescence intensity was observed (Figure 2b). The above changes might be attributed to the loss of conjugation in the photoproduct (**2**) due to the Photo-Favorskii rearrangement[18] (Scheme 1). Further, we investigated the photouncaging process by the ^{1}H NMR study (Figure S19).[18] We irradiated Lyso-Naph-Cbl in the DMSO-d_6/D_2O binary mixture with visible light at regular time intervals. From the ^{1}H NMR study, we noted the formation of the rearranged photoproduct and release of chlorambucil (Figure S19).

A similar photouncaging study of Lyso-Naph-Cbl was also carried out at lysosomal pH. We noted faster uncaging (20 min) at lower pH = 5.4 (Figure S18a), which is a characteristic of the Photo-Favorskii rearrangement.[13,18] The quantum yield of photouncaging (ϕ_u) at different pH values was calculated by potassium ferrioxalate actinometery[28] and found to be 0.19 and 0.24 at pH 7.4 and 5.4, respectively.

Mechanism of Photorelease from Lyso-Naph-Cbl. Based on the above experimental findings, literature reports,[13,19,29] and our recent work on the 2-hydroxy-6-napthacyl phototrigger,[18] we proposed a possible mechanism of photouncaging of Lyso-Naph-Cbl (Scheme 3). Upon irradiation, Lyso-Naph-Cbl gets excited to its singlet excited state **8** where it undergoes a rapid ESIPT process and generates a zwitterionic form **9**, which then undergoes efficient intersystem crossing (ISC) to its triplet excited state **10**. A Photo-Favorskii-type rearrangement occurs from the triplet state to form a putative intermediate **11** and subsequent release of chlorambucil. Finally, water reacts with the putative intermediate, resulting in the formation of the photoproduct (**2**). Further, the formation of the photoproduct (**2**) and released chlorambucil (**3**) was confirmed by HRMS (Figures S20−S22).

We carried out different sets of experiments to prove that the reaction proceeds via a triplet state. At first, we carried out the photolysis of Lyso-Naph-Cbl (1×10^{-4} M) in acetonitrile/

https://doi.org/10.1021/acsami.1c19022
ACS Appl. Mater. Interfaces 2022, 14, 4862−4870

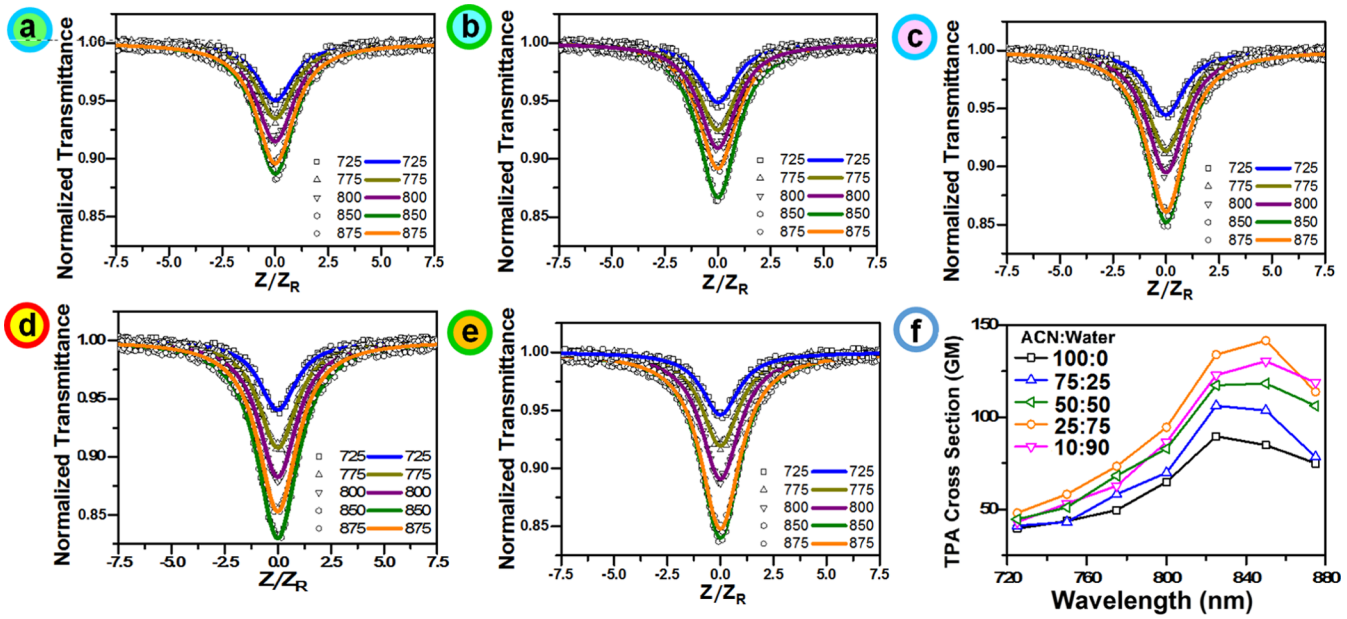

Figure 3. (a–e) OA *z*-scan curves recorded at different wavelengths using a 10^{-4} M solution of Lyso-Naph-Cbl in the ACN/PBS buffer binary mixture with varying water fractions (f_w). (f) Comparison of the TPA cross section of Lyso-Naph-Cbl at different wavelengths and in different f_w.

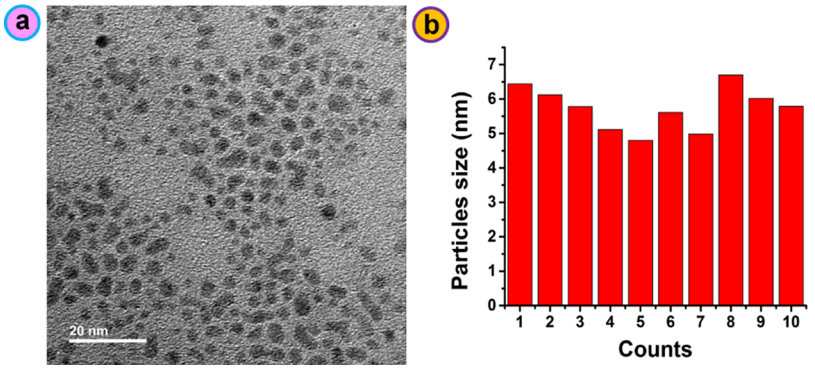

Figure 4. (a) TEM image of Lyso-Naph-Cbl-NPs. (b) Average size of Lyso-Naph-Cbl-NPs.

PBS buffer of pH 7.4 (f_w = 95%) in the presence and absence of 0.2 mM triplet quencher potassium sorbate (PoS).[18,19] The result showed that drug release by Lyso-Naph-Cbl was almost completely arrested in the presence of 0.2 mM PoS, clearly indicating that photorelease occurs from the triplet excited state (Figure S23). Next, we examine the photouncaging in the presence and absence of aerated oxygen. We found that the photochemical quantum yield is less in the presence of aerated oxygen (ϕ_u = 0.15). This decrease in the photochemical quantum yield in aerated oxygen is due to the possible energy transfer from the triplet state of Lyso-Naph-Cbl to oxygen. Therefore, the above-mentioned observations indicate that the photolysis occurred from the triplet state.

Measurement of TPA Cross Section (δ_a) of Lyso-Naph-Cbl. Next, we investigated the two-photon absorption ability of Lyso-Naph-Cbl. Using a single-beam open-aperture (OA) *z*-scan technique,[30] we performed the nonlinear optical measurement of Lyso-Naph-Cbl. A Ti: Sapphire laser giving 100 fs pulses with 1 W average power and a focused beam spot size of 50 μm was used for the OA *z*-scan technique. OA *z*-scan measurements were carried out on 10^{-4} M solutions of Lyso-Naph-Cbl in ACN/PBS buffer (pH 7.4) binary mixtures with varying water fractions (f_w) at different wavelengths, ranging from 700–850 nm (Figure 3).

The experimental OA curves were then fitted with the transmission equation, including two-photon absorption (TPA).[30] The TPA cross section (δ_a) of Lyso-Naph-Cbl was then calculated[31] and is summarized in Table S2 and Figure 3f. From Table S2, we noticed that our DDS has a good TPA cross section in the NIR region. The highest value of δ_a for Lyso-Naph-Cbl was obtained at 850 nm, which was 142 GM (1 GM = 10^{-50} cm^4 s/photon/molecule). We calculated the two-photon uncaging cross section (δ_u) to understand the efficacy of drug release by two-photon irradiation. We used single photon ϕ_u to calculate δ_u by the equation $\delta_u = \phi_u\delta_a$.[27] The highest δ_u values for our DDS obtained at 850 nm were 27 and 34 GM at pH 7.4 and 5.4, respectively.

Two-Photon Uncaging of Chlorambucil from Lyso-Naph-Cbl. The two-photon uncaging of Lyso-Naph-Cbl was demonstrated at two different pH values, 7.4 and 5.4. A 300 μL (10^{-4} M) solution of Lyso-Naph-Cbl in f_w = 95% ACN/PBS buffer was irradiated with a 100 fs pulsed laser with a focused beam size of 50 μm and an average power of 800 mW at a wavelength of 850 nm. The released chlorambucil was quantified from the HPLC study and found that 24 and 29%

https://doi.org/10.1021/acsami.1c19022
ACS Appl. Mater. Interfaces 2022, 14, 4862–4870

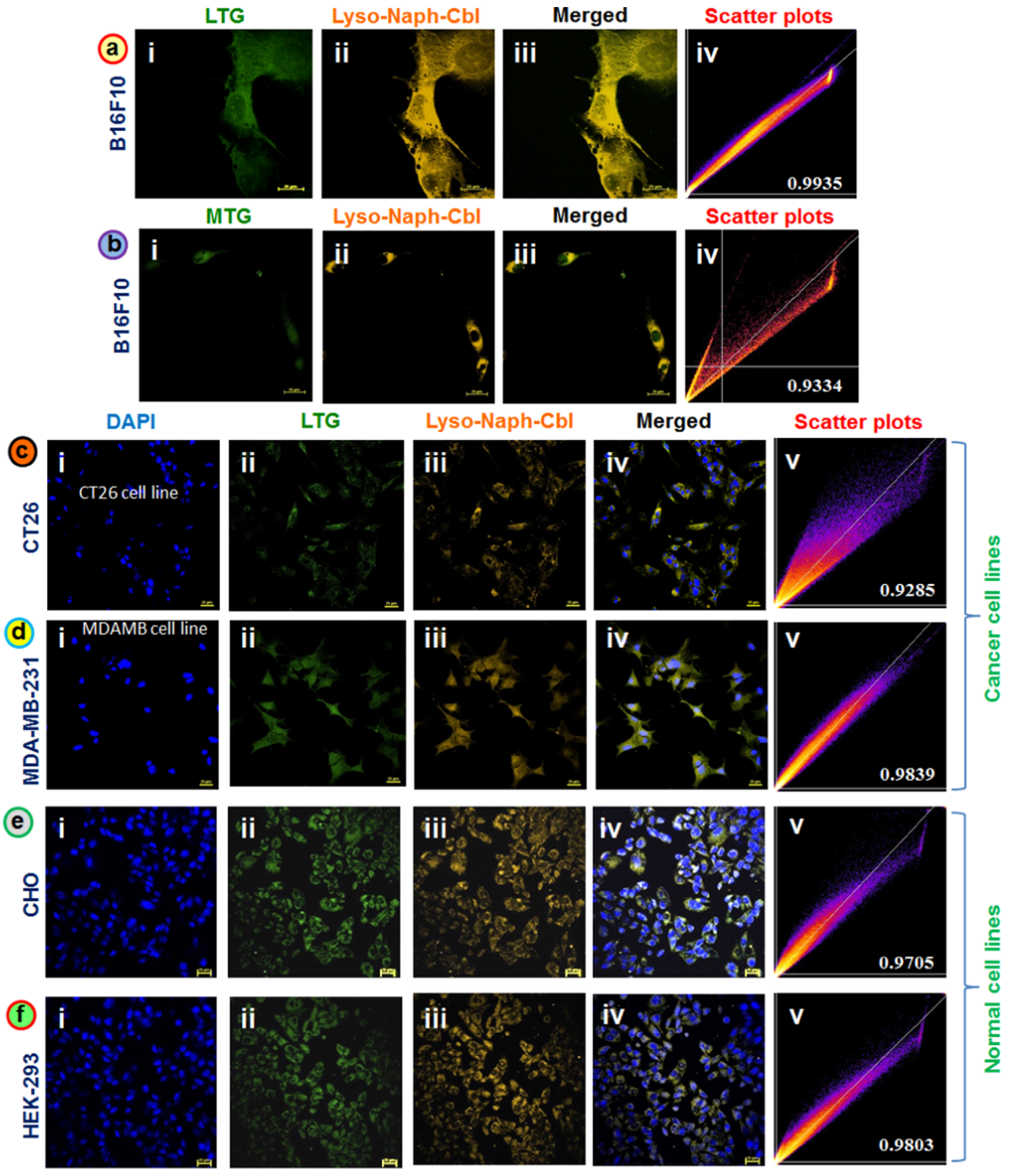

Figure 5. (a) Live B16F10 cell lines treated with LTG and Lyso-Naph-Cbl-NPs and CLSM images were collected via [a(i)] green channel, [a(ii)] yellow channel, [a(iii)] merged image of green and yellow channels, and [a(iv)] scatter plot and Pearson's correlation coefficient. (b) B16F10 cell lines treated with MTG and Lyso-Naph-Cbl-NPs and CLSM images were collected via [b(i)] green channel, [b(ii)] yellow channel, [b(iii)] merged image of green and yellow channels, and [b(iv)] scatter plot and Pearson's correlation coefficient. CT26 (c), MDA-MB-231 (d), CHO (e), and HEK-293 (f) cell lines treated with DAPI, LTG, and Lyso-Naph-Cbl-NPs, and CLSM images were collected via (i) blue channel, (ii) green channel, (iii) yellow channel, (iv) merged image of blue, green, and yellow channels, and (v) scatter plot and Pearson's correlation coefficient.

of the drug was released after 3 h of irradiation at pH 7.4 and 5.4, respectively.

***In Vitro* Applicability of Lyso-Naph-Cbl as Nano-DDS.** The positive outcome of our DDS encouraged us to investigate its targeting, imaging, and drug release capability by *in vitro* studies using cancer cell lines.

At first, we prepared pure organic nanoparticles (NPs) of Lyso-Naph-Cbl by the reprecipitation technique by following our previously reported procedure for biological application (Figure 4a).[32] To find the size and shape of Lyso-Naph-Cbl-NPs, we took transmission electron microscopy (TEM) image. Figure 4a,b reveals that Lyso-Naph-Cbl-NPs are almost spherical, with an average size of ~6 nm.

Next, we examined the targeting and cell imaging potential of our nano-DDS using cancerous cell line B16F10. To understand its cytoplasmic distribution, Lyso-Naph-Cbl-NPs were counterstained with LysoTracker Green (LTG) and MitoTracker Green (MTG) separately. The confocal laser scanning microscopy (CLSM) images (Figure 5a,b) showed that Lyso-Naph-Cbl-NPs are mainly colocalized with LTG (Figure 5a) but not with MTG (Figure 5b). Pearson's correlation coefficients for the colocalization of Lyso-Naph-

https://doi.org/10.1021/acsami.1c19022
ACS Appl. Mater. Interfaces 2022, 14, 4862−4870

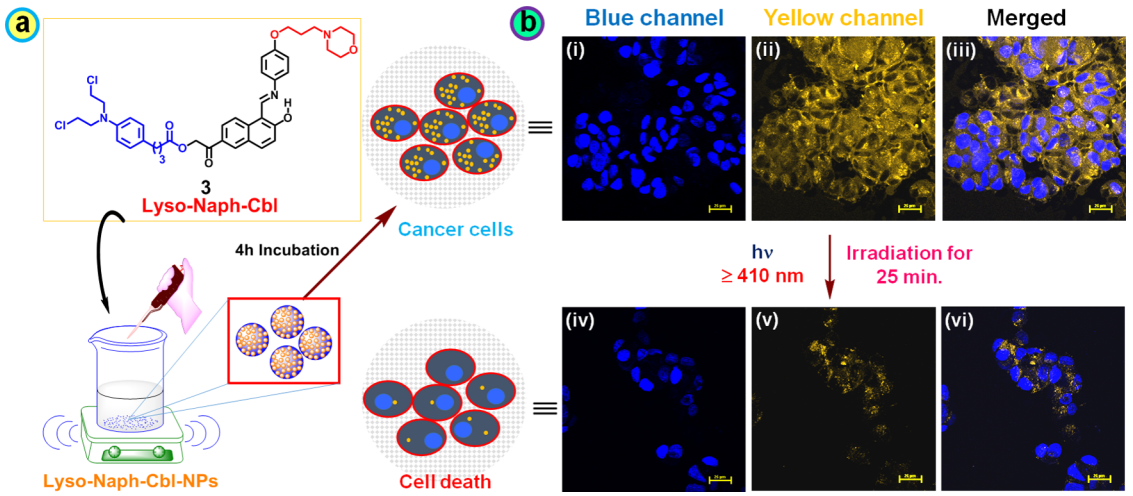

Figure 6. (a) Schematic representation of the preparation of Lyso-Naph-Cbl-NPs; (b) B16F10 cell lines treated with DAPI and Lyso-Naph-Cbl-NPs and CLSM images were collected before irradiation via [b(i)] blue channel, [b(ii)] yellow channel, and [b(iii)] merged image of blue and yellow channels and after irradiation via [b(iv)] blue channel, [b(v)] yellow channel, and [b(vi)] merged image of blue and yellow channels.

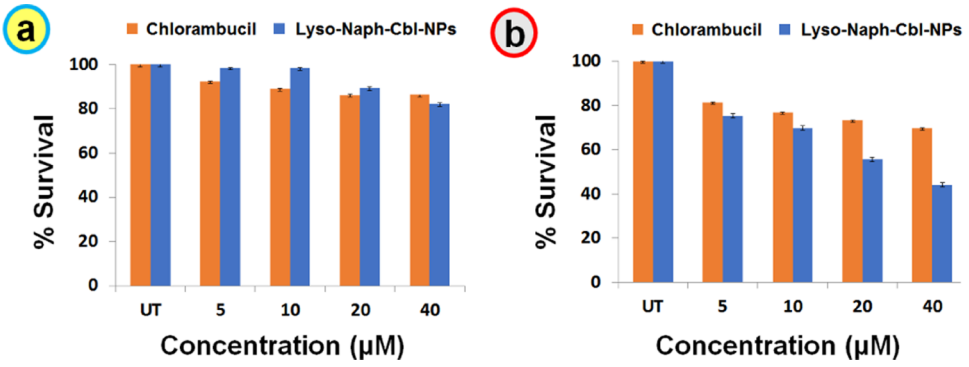

Figure 7. Cell viability assays for Lyso-Naph-Cbl-NPs and free chlorambucil with the B16F10 cell line (a) in the dark and (b) after light irradiation for 25 min.

Cbl-NPs with LTG and MTG were found to be 0.9935 and 0.9334, respectively. Furthermore, extensive colocalization of Lyso-Naph-Cbl-NPs in the lysosome (Figure 5a-IV) over mitochondria (Figure 5b-IV) was confirmed by scatter plots. Concentrated pixels along the diagonals of the corresponding scatter plot indicate a high degree of colocalization with LTG. To further explore the lysosome targeting ability of Lyso-Naph-Cbl-NPs, we carried out the colocalization study with two different cancer cell lines, CT26 (Figure 5c) and MDA-MB-231 (Figure 5d), and two different normal cell lines, CHO (Figure 5e) and HEK-293 (Figure 5f). We counterstained each cell line with 4,6-diamidino-2-phenylindole (DAPI), Lyso-Tracker Green (LTG), and Lyso-Naph-Cbl-NPs separately. The corresponding Pearson's correlation coefficient and scatter plots indicate extensive colocalization with LTG.

After the cellular internalization study of Lyso-Naph-Cbl-NPs, we investigated the *in vitro* drug uncaging ability of our nano-DDS by light irradiation. B16F10 was incubated with Lyso-Naph-Cbl-NPs, and the cell nuclei were stained with DAPI. After 1 h of incubation, we irradiated the cells with visible light ($\lambda \geq 410$ nm) for 25 min. CLSM images (Figure 6b) showed that before irradiation, Lyso-Naph-Cbl-NPs exhibited intense fluorescence color (Figure 6b-ii). After irradiation for 25 min, the fluorescence intensity decreased sharply (Figure 6b-v), which validates the photoresponsive drug delivery within the lysosome of the cells. To confirm the cytosolic drug delivery, the degree of the cellular uptake of Lyso-Naph-Cbl-NPs and colorimetric differences before and after photolysis were also assessed quantitatively *in vitro* by flow cytometry using B16F10 cell lines (Figure S24).

Then, we carried out the cytotoxicity study with Lyso-Naph-Cbl-NPs by the MTT assay (MTT = 3-(4,5-dimethylthiazol-2-yl)-2,5-diphenyltetrazolium bromide, a yellow tetrazole) using cancerous cell line B16F10. We found above 80% cell viability at different concentrations of Lyso-Naph-Cbl (Figure 7a). Next, we irradiated the Lyso-Naph-Cbl-NP-treated B16F10 cells with visible light and found the enhanced cytotoxicity of Lyso-Naph-Cbl-NPs compared to free chlorambucil (Figure 7b). The enhanced cytotoxicity can be explained by the cytosolic drug delivery, validated by MTT data.

CONCLUSIONS

In summary, for the first time, we developed an organelle-targeted two-photon NIR light-responsive DDS based on the naphthalene chromophore. The DDS was converted into pure organic nanoparticles, targeting the lysosome and releasing the drug molecule inside the cancerous cells upon irradiation. Interestingly, our nano-DDS showed real-time monitoring of the drug release by a sharp decrease in fluorescence intensity. Finally, the nano-DDS exhibited enhanced cytotoxicity compared to free chlorambucil due to cytosolic drug delivery. Our phototrigger can be utilized to design DDS for targeting

https://doi.org/10.1021/acsami.1c19022
ACS Appl. Mater. Interfaces 2022, 14, 4862−4870

other organelles by changing the targeting moiety via simple synthetic modifications.

EXPERIMENTAL SECTION

Photolysis of Lyso-Naph-Cbl. A 40 mL (1×10^{-4} M) solution of Lyso-Naph-Cbl in acetonitrile/PBS buffer of pH 7.4 ($f_w = 95$) was taken and degassed prior to exposure to a medium pressure mercury lamp (125 W) as the source of light ($\lambda \geq 410$ nm) using a 1 M aqueous solution of $NaNO_2$ UV cutoff filter.

Two-Photon Photolysis. The two-photon uncaging of Lyso-Naph-Cbl was demonstrated with two different solutions of pH 7.4 and 5.4. A 300 μL (1×10^{-4} M) solution of Lyso-Naph-Cbl in (f_w = 95%) acetonitrile/PBS buffer of pH 7.4 and 5.4 was irradiated with a 100 fs pulsed laser with 50 μm focal beam size and 800 mW average power at a wavelength of 850 nm. Small aliquots (25 μL) before and after the photolysis were taken out from the solution for the HPLC study. The released drug was quantified from the HPLC peak area in comparison with an injected authentic sample.

Preparation of Nanoparticles of Lyso-Naph-Cbl. Lyso-Naph-Cbl was dissolved in tetrahydrofuran (THF) to prepare a 1×10^{-3} M solution. Next, 25 μL of the solution was added dropwise (1 drop per minute) via a syringe into 2.5 mL of water in a glass vial with constant sonication. Sonication was continued for 30 min at room temperature. Then, the vial was heated to 37 °C, and nitrogen was purged through the solution for 1 h to remove THF to give a 1×10^{-5} M solution of Lyso-Naph-Cbl-NPs.

Cell Lines. Cancerous cell lines B16F10 (melanoma), MDA-MB-231 (human breast adenocarcinoma), and CT26 (Mus musculus colon carcinoma) and the non-cancerous cell lines HEK-293 (human embryonic kidney 293) and CHO (Chinese hamster ovary) were obtained from the National Centre for Cell Science (NCCS), Pune, India. All of the cell lines were cultured in Dulbecco's modified Eagle's medium (DMEM, Gibco) supplemented with 10% fetal bovine serum, 1% nonessential amino acid, 1% streptomycin, 1% L-glutamine, and 1% penicillin. All cells were cultured at 37 °C in a CO_2 incubator (Thermo Fisher Scientific).

Intracellular Distribution of Lyso-Naph-Cbl-NPs in Cancerous Cell Line B16F10. Intracellular localization of Lyso-Naph-Cbl-NPs by the cancerous B16F10 cell line was monitored by confocal laser scanning microscopy (CLSM). The cells were cultured following the standard protocols and were incubated with Lyso-Naph-Cbl-NPs (10 μM in HEPES buffer) under 5% CO_2 at humified conditions at 37 °C for 4 h. Cell mitochondria and lysosomes were stained separately with MitoTracker Green (MTG) and LysoTracker Green (LTG), respectively. Then imaging was done using a Nikon confocal microscope (Eclipse Ti-E) using a respective filter.

Intracellular distribution of Lyso-Naph-Cbl-NPs in cancerous cell lines MDA-MB-231 and CT26 and non-cancerous cell lines CHO and HEK-293. All cell lines were cultured following the standard protocols and were incubated with Lyso-Naph-Cbl-NPs (10 μM in HEPES buffer) under 5% CO_2 at humified conditions at 37 °C for 4 h. The cell lines were counterstained with 4,6-diamidino-2-phenylindole (DAPI) and LysoTracker Green (LTG), respectively. Then, imaging was done using a Nikon confocal microscope (Eclipse Ti-E) using a separate filter.

Fluorogenic Real-Time Monitoring of the Drug Release Study with B16F10 Cell Lines. B16F10 cell lines were cultured following the standard protocols and were treated with Lyso-Naph-Cbl-NPs (10 μM in HEPES buffer), and cell nuclei were stained with 4,6-diamidino-2-phenylindole (DAPI). The cells were incubated at 37 °C under 5% CO_2 at humified conditions for 4 h. After that, the cells were irradiated with visible light (≥410 nm) for 25 min. Fluorescent images were captured before and after the irradiation using a confocal microscope (Nikon Ti Eclipse).

***In Vitro* Cell Viability Assay.** The *in vitro* cytotoxic studies of Lyso-Naph-Cbl-NPs and the free drug chlorambucil (Cbl) were carried out using the MTT (3-(4,5- dimethylthiazole-2-yl)-2,5-diphenyltetrazolium bromide) assay. Briefly, cancerous cell line B16F10 was grown in their log phase. The cells were seeded in 96-well plates in Dulbecco's modified Eagle's medium (DMEM) containing 10% fetal bovine serum (FBS) for 8 h. The cell lines were then incubated with different concentrations (5–40 μM) of Lyso-Naph-Cbl-NPs and Cbl separately in HEPES buffer, at 37 °C in 5% CO_2 for 4 h. Next, we irradiated these cells with visible light for 25 min and incubated them for 72 h. Then, cytotoxicity was measured using the MTT assay before and after light irradiation.

Cellular Uptake Study with Flow Cytometry. The degree of cellular uptake was studied quantitatively by flow cytometry. B16F10 cell lines were cultured in 6-well plates at a density of 1×10^5 cells per well for 8 h. The cells were then incubated in two different sets with Lyso-Naph-Cbl-NPs (10 μM), harvested by trypsinization, and washed with PBS (3 × 1 mL). One set was irradiated with visible light ($\lambda \geq 410$ nm) for 25 min among the two sets. Cellular uptakes before and after irradiation were analyzed using a flow cytometer (BD FACS canto II) under the PE channel. The shift of the fluorescently labeled cells was compared with untreated cells using FCS software.

ASSOCIATED CONTENT

Supporting Information

The Supporting Information is available free of charge at https://pubs.acs.org/doi/10.1021/acsami.1c19022.

Synthetic details; ^{1}H NMR, ^{13}C NMR, and HRMS spectra; experimental details of UV–vis spectroscopy; solid-state emission spectrum of Lyso-Naph-Cbl; measurement of fluorescence quantum yields; stability study; quantification of the released drug from Lyso-Naph-Cbl; measurement of photochemical quantum yields; triplet quenching study; *Z*-scan measurement; calculation of TPA cross section of Lyso-Naph-Cbl; and flow cytometry analysis (PDF)

AUTHOR INFORMATION

Corresponding Authors

Avijit Jana − *Department of Organic Synthesis and Process Chemistry, CSIR-Indian Institute of Chemical Technology Hyderabad, Hyderabad 500007, India; Academy of Scientific and Innovative Research (AcSIR), Ghaziabad 201002, India;* orcid.org/0000-0002-4828-2970; Email: avijit@iict.res.in

N. D. Pradeep Singh − *Department of Chemistry, Indian Institute of Technology Kharagpur, Kharagpur 721302, India;* orcid.org/0000-0001-6806-9774; Email: ndpradeep@chem.iitkgp.ac.in

Authors

Biswajit Roy − *Department of Chemistry, Indian Institute of Technology Kharagpur, Kharagpur 721302, India;* orcid.org/0000-0001-5217-4270

Rakesh Mengji − *Department of Organic Synthesis and Process Chemistry, CSIR-Indian Institute of Chemical Technology Hyderabad, Hyderabad 500007, India; Academy of Scientific and Innovative Research (AcSIR), Ghaziabad 201002, India*

Samrat Roy − *Department of Physics, Indian Institute of Science Education and Research Kolkata, Mohanpur, West Bengal 741246, India;* orcid.org/0000-0002-5461-8418

Bipul Pal − *Department of Physics, Indian Institute of Science Education and Research Kolkata, Mohanpur, West Bengal 741246, India;* orcid.org/0000-0002-1415-2326

Complete contact information is available at: https://pubs.acs.org/10.1021/acsami.1c19022

https://doi.org/10.1021/acsami.1c19022
ACS Appl. Mater. Interfaces 2022, 14, 4862−4870

Notes

The authors declare no competing financial interest.

■ ACKNOWLEDGMENTS

The authors thank DST SERB (Grant Nos. EMR/2016/005885 and SERB/F/6429/2020-21) for financial support. A.J. is thankful to SERB for the research grant SB/SRS/2020-21/35/CS. The CSIR-IICT Communication number for this manuscript is IICT/Pubs./2021/196.

■ REFERENCES

(1) de Duve, C.; Pressman, B. C.; Gianetto, R.; Wattiaux, R.; Appelmans, F. Tissue Fractionation Studies. 6. Intracellular Distribution Patterns of Enzymes in Rat-Liver Tissue. *Biochem. J.* **1955**, *60*, 604−617.

(2) Zhu, H.; Fan, J.; Du, J.; Peng, X. Fluorescent Probes for Sensing and Imaging within Specific Cellular Organelles. *Acc. Chem. Res.* **2016**, *49*, 2115−2126.

(3) Xu, W.; Zeng, Z.; Jiang, J.-H.; Chang, Y.-T.; Yuan, L. Discerning the Chemistry in Individual Organelles with Small-Molecule Fluorescent Probes. *Angew. Chem., Int. Ed.* **2016**, *55*, 13658−13699.

(4) Sakhrani, N. M.; Padh, H. Organelle Targeting: Third Level of Drug Targeting. *Drug Des., Dev. Ther.* **2013**, *7*, 585−599.

(5) Dielschneider, R. F.; Henson, E. S.; Gibson, S. B. Lysosomes as Oxidative Targets for Cancer Therapy. *Oxid. Med. Cell. Longevity* **2017**, *2017*, 1−8.

(6) Hu, F.; Liu, B. Organelle-Specific Bioprobes Based on Fluorogens with Aggregation-Induced Emission (AIE) Characteristics. *Org. Biomol. Chem.* **2016**, *14*, 9931−9944.

(7) Li, Y.-J.; Lei, Y.-H.; Yao, N.; Wang, C.-R.; Hu, N.; Ye, W.-C.; Zhang, D.-M.; Chen, Z.-S. Autophagy and Multidrug Resistance in Cancer. *Chin. J. Cancer.* **2017**, *36*, No. 52.

(8) Manchun, S.; Dass, C. R.; Sriamornsak, P. Targeted Therapy for Cancer Using pH-Responsive Nanocarrier Systems. *Life Sci.* **2012**, *90*, 381−387.

(9) He, X.; Li, J.; An, S.; Jiang, C. pH-Sensitive Drug-Delivery Systems for Tumor Targeting. *Ther. Delivery* **2013**, *4*, 1499−1510.

(10) Dong, H.; Pang, L.; Cong, H.; Shen, Y.; Yu, B. Application and Design of Esterase-Responsive Nanoparticles for Cancer Therapy. *Drug Delivery* **2019**, *26*, 416−432.

(11) Cao, Z.; Li, W.; Liu, R.; Li, X.; Li, H.; Liu, L.; Chen, Y.; Lv, C.; Liu, Y. pH- and Enzyme-Triggered Drug Release as an Important Process in the Design of Anti-Tumor Drug Delivery Systems. *Biomed. Pharmacother.* **2019**, *118*, No. 109340.

(12) de la Rica, R.; Aili, D.; Stevens, M. M. Enzyme-Responsive Nanoparticles for Drug Release and Diagnostics. *Adv. Drug Delivery Rev.* **2012**, *64*, 967−978.

(13) Klán, P.; Šolomek, T.; Bochet, C. G.; Blanc, A.; Givens, R.; Rubina, M.; Popik, V.; Kostikov, A.; Wirz, J. Photoremovable Protecting Groups in Chemistry and Biology: Reaction Mechanisms and Efficacy. *Chem. Rev.* **2013**, *113*, 119−191.

(14) Feng, S.; Harayama, T.; Chang, D.; Hannich, J. T.; Winssinger, N.; Riezman, H. Lysosome-Targeted Photoactivation Reveals Local Sphingosine Metabolism Signatures. *Chem. Sci.* **2019**, *10*, 2253−2258.

(15) Kand, D.; Pizarro, L.; Angel, I.; Avni, A.; Friedmann-Morvinski, D.; Weinstain, R. Organelle-Targeted BODIPY Photocages: Visible-Light-Mediated Subcellular Photorelease. *Angew. Chem., Int. Ed.* **2019**, *58*, 4659−4663.

(16) Piant, S.; Bolze, F.; Specht, A. Two-photon Uncaging, From Neuroscience to Materials. *Opt. Mater. Express* **2016**, *6*, 1679−1691.

(17) Abe, M.; Chitose, Y.; Jakkampudi, S.; Thuy, P.; Lin, Q.; Van, B.; Yamada, A.; Oyama, R.; Sasaki, M.; Katan, C. Design and Synthesis of Two-Photon Responsive Chromophores for Near-Infrared Light-Induced Uncaging Reactions. *Synthesis* **2017**, *49*, 3337−3346.

(18) Roy, B.; Kundu, M.; Singh, A. K.; Singha, T.; Bhattacharya, S.; Datta, P. K.; Mandal, M.; Singh, N. D. P. Stepwise Dual Stimuli Triggered Dual Drug Release by a Single Naphthalene Based Two-Photon Chromophore to Reverse MDR for Alkylating Agents with Dual Surveillance in Uncaging Steps. *Chem. Commun.* **2019**, *55*, 13140−13143.

(19) Barman, S.; Mukhopadhyay, S. K.; Biswas, S.; Nandi, S.; Gangopadhyay, M.; Dey, S.; Anoop, A.; Pradeep Singh, N. D. A *p*-Hydroxyphenacyl−Benzothiazole−Chlorambucil Conjugate as a Real-Time-Monitoring Drug-Delivery System Assisted by Excited-State Intramolecular Proton Transfer. *Angew. Chem., Int. Ed.* **2016**, *55*, 4194−4198.

(20) Chen, L.; Wu, D.; Kim, J.-M.; Yoon, J. An ESIPT-Based Fluorescence Probe for Colorimetric, Ratiometric, and Selective Detection of Phosgene in Solutions and the Gas Phase. *Anal. Chem.*, **2017**, *89*, 12596−12601.

(21) Sedgwick, A. C.; Wu, L.; Han, H.-H.; Bull, S. D.; He, X.-P.; James, T. D.; Sessler, J. L.; Tang, B. Z.; Tian, H.; Yoon, J. Excited-State Intramolecular Proton-Transfer (ESIPT) Based Fluorescence Sensors and Imaging Agents. *Chem. Soc. Rev.* **2018**, *47*, 8842−8880.

(22) Gao, M.; Hu, Q.; Feng, G.; Tang, B. Z.; Liu, B. A Fluorescent Light-Up Probe with "AIE + ESIPT" Characteristics for Specific Detection of Lysosomal Esterase. *J. Mater. Chem. B* **2014**, *2*, 3438−3442.

(23) Mei, J.; Leung, N. L. C.; Kwok, R. T. K.; Lam, J. W. Y.; Tang, B. Z. Aggregation-Induced Emission: Together We Shine, United We Soar! *Chem. Rev.* **2015**, *115*, 11718−11940.

(24) Chen, Y.; Fang, Y.; Gu, H.; Qiang, J.; Li, H.; Fan, J.; Cao, J.; Wang, F.; Lu, S.; Chen, X. Color-Tunable and ESIPT-Inspired Solid Fluorophores Based on Benzothiazole Derivatives: Aggregation-Induced Emission, Strong Solvatochromic Effect, and White Light Emission. *ACS Appl. Mater. Interfaces* **2020**, *12*, 55094−55106.

(25) Ni, J.-S.; Lee, M. M. S.; Zhang, P.; Gui, C.; Chen, Y.; Wang, D.; Yu, Z.-Q.; Kwok, R. T. K.; Lam, J. W. Y.; Tang, B. Z. Swiss Knife-Inspired Multifunctional Fluorescence Probes for Cellular Organelle Targeting Based on Simple AIEgens. *Anal. Chem.* **2019**, *91*, 2169−2176.

(26) Song, H.; Lee, Y. S.; Roh, E. J.; Seo, J. H.; Oh, K.-S.; Lee, B. H.; Han, H.; Shin, K. J. Discovery of Potent and Selective Rhodanine Type IKKβ Inhibitors by Hit-to-Lead Strategy. *Bioorg. Med. Chem. Lett.* **2012**, *22*, 5668−5674.

(27) Roy, B.; Roy, S.; Kundu, M.; Maji, S.; Pal, B.; Mandal, M.; Singh, N. D. P. Ground-State Proton-Transfer (GSPT)-Assisted Enhanced Two-Photon Uncaging from a Binol-based AIE-Fluorogenic Phototrigger. *Org. Lett.* **2021**, *23*, 2308−2313.

(28) Demas, J. N.; Bowman, W. D.; Zalewski, E. F.; Velapoldi, R. A. Determination of the Quantum Yield of the Ferrioxalate Actinometer with Electrically Calibrated Radiometers. *J. Phys. Chem. A* **1981**, *85*, 2766−2771.

(29) Givens, R. S.; Heger, D.; Hellrung, B.; Kamdzhilov, Y.; Mac, M.; Conrad, P. G.; Cope, E.; Lee, J. I.; Mata-Segreda, J. F.; Schowen, R. L.; Wirz, J. The Photo-Favorskii Reaction of *p*-Hydroxyphenacyl Compounds is Initiated by Water-Assisted, Adiabatic Extrusion of a Triplet Biradical. *J. Am. Chem. Soc.* **2008**, *130*, 3307−3309.

(30) Sheik-Bahae, M.; Said, A. A.; Wei, T.-H.; Hagan, D. J.; Van Stryland, E. W. Sensitive Measurement of Optical Nonlinearities Using a Single Beam. *IEEE J. Quantum Electron.* **1990**, *26*, 760−769.

(31) Ajami, A.; Husinsky, W.; Liska, R.; Pucher, N. Two-Photon Absorption Cross Section Measurements of Various Two-Photon Initiators for Ultrashort Laser Radiation Applying the Z-Scan Technique. *J. Opt. Soc. Am. B* **2010**, *27*, 2290−2297.

(32) Jana, A.; Devi, K. S. P.; Maiti, T. K.; Singh, N. D. P. Perylene-3-Ylmethanol: Fluorescent Organic Nanoparticles as a Single-Component Photoresponsive Nanocarrier with Real-Time Monitoring of Anticancer Drug Release. *J. Am. Chem. Soc.* **2012**, *134*, 7656−7659.

https://doi.org/10.1021/acsami.1c19022
ACS Appl. Mater. Interfaces 2022, 14, 4862−4870